

Extraordinary Optical Transmission Brightens Near-Field Fiber Probe

Lars Neumann,[†] Yuanjie Pang,[§] Amel Houyou,[†] Mathieu L. Juan,[†] Reuven Gordon,[§] and Niek F. van Hulst^{*,†,‡}

[†]ICFO-Institut de Ciències Fotoniques, Mediterranean Technology Park, 08860 Castelldefels (Barcelona), Spain

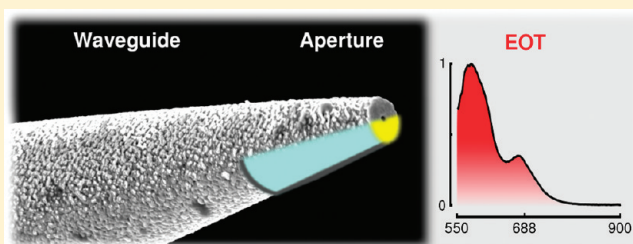
[‡]ICREA-Institució Catalana de Recerca i Estudis Avançats, 08015 Barcelona, Spain

[§]Department of Electrical and Computer Engineering, University of Victoria, Victoria, British Columbia V8W 3P6, Canada

ABSTRACT: Near-field scanning optical microscopy (NSOM) offers high optical resolution beyond the diffraction limit for various applications in imaging, sensing, and lithography; however, for many applications the very low brightness of NSOM aperture probes is a major constraint. Here, we report a novel NSOM aperture probe that gives a 100× higher throughput and 40× increased damage threshold than conventional near-field aperture probes. These brighter probes facilitate near-field imaging of single molecules with apertures as small as 45 nm in diameter.

We achieve this improvement by nanostructuring the probe and by employing a novel variant of extraordinary optical transmission, relying solely on a single aperture and a coupled waveguide. Comprehensive electromagnetic simulations show good agreement with the measured transmission spectra. Due to their significantly increased throughput and damage threshold, these resonant configuration probes provide an important step forward for near-field applications.

KEYWORDS: Extraordinary optical transmission, near-field scanning optical microscopy, nanophotonics, nanoplasmonics, nanoimaging, waveguide resonance, focused ion beam



Near-field scanning optical microscopy (NSOM) combines optical microscopy with scanning probe microscopy to achieve an optical resolution well beyond the diffraction limit. Its high resolution has found many applications in fields as optical imaging,^{1,2} material science,^{3–6} and nanolithography.^{7–9} Technically, a NSOM probe is usually realized by a single, subwavelength aperture that is formed by tapering an optical fiber and coating its side walls to prevent light leakage. However, the drawback of subwavelength apertures is their very limited throughput. Bethe's theory for optical transmission through a subwavelength aperture in a metal screen gives a steep fourth-power reduction in the transmission with the aperture diameter, necessitating a trade-off between resolution and brightness.¹⁰ Apart from the transmission through the aperture, the absolute throughput is limited by the low damage threshold of conventional near-field probes. Here, the light delivery through the taper to the aperture depends greatly on the actual taper shape, its length, and the quality of the metal layer (aluminum) preventing light leakage. These limitations result in an optical throughput of near-field probes of typically only 10^{-5} to 10^{-7} .^{11–13}

Many approaches have been explored to improve the coupling through subwavelength apertures. The transmission through a single aperture was enhanced by reshaping the aperture.^{14–16} Aperture arrays have shown extraordinary optical transmission (EOT),¹⁷ and related to EOT is the beaming of light from single apertures flanked with a periodic structure.¹⁸ Reshaping and grating structures have only been demonstrated in thin, extended

films, which are also required for the aperture arrays in standard EOT. Essential for NSOM, however, is a tiny end face that, similar to atomic force microscopy, interacts with the sample and is directly responsible for resolution and sensitivity. Thus, the aforementioned approaches do not provide a practical solution. Alternatively, "apertureless" NSOM employs a sharp tip or nanoparticle to concentrate the electric field and thus provides this tiny end face;¹⁹ however, as apertureless probes are excited from the far-field, modulation schemes are necessary to overcome the strong background illumination.²⁰ Few approaches have been made to enhance transmission and brightness while maintaining resolution and applicability as an aperture NSOM probe. Among those are the incorporation of antenna structures with the aperture^{21,22} or a photonic crystal²³ and the excitation of plasmons along and inside the probe.^{24,25}

In this report we demonstrate a NSOM probe that offers both improved absolute throughput and efficient coupling through the aperture and thus allows sufficient brightness to image single molecules with an aperture of 45 nm diameter. We have implemented an alternative realization of EOT that does not require an array of apertures or a grating structure;^{26–28} instead, it uses resonant coupling to the adjacent waveguide. So far, this waveguide resonance EOT (WR-EOT) has only been demonstrated

Received: July 29, 2010

Revised: October 30, 2010

Published: December 22, 2010

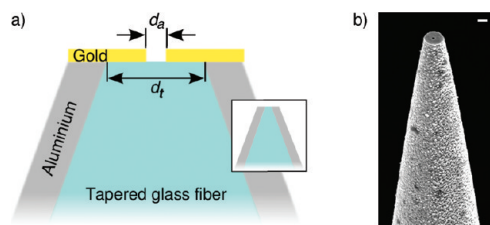


Figure 1. Schematic and SEM image of the EOT near-field fiber probe. (a) The fiber is tapered and then coated with a 220 nm aluminum layer to prevent light leakage. We adjust the final taper diameter d_t , which determines the resonant TM mode cutoff-wavelength, by focused ion beam (FIB) milling. The aperture with diameter d_a is milled into a 90 nm gold layer that is evaporated onto the end face. Inset: Conventional NSOM fiber. (b) The SEM image shows the final configuration with an aperture of diameter $d_a = 110$ nm. The scale bar is 500 nm.

for coupling between two waveguides and the microwave regime.²⁹ Here, we demonstrate a nanoscale version WR-EOT providing enhanced transmission through a NSOM probe at visible to near-IR wavelengths. By varying the geometry of the fiber optic waveguide, we demonstrate tuning of the transmission resonance wavelength from 600 to 900 nm. Comprehensive electromagnetic simulations confirm that energy resonantly stored in the waveguide above a single mode's cutoff wavelength is responsible for the WR-EOT. We also show that the absolute throughput is enhanced by this nanostructuring of the tapered fiber. While these probes have a slightly wider base than conventional metal-coated tapered fiber probes, they show 40 \times improvement in the optical damage threshold and a 100 \times enhancement in throughput.

Figure 1a shows a schematic and Figure 1b a side view scanning electron microscopy (SEM) image of the metal-coated tapered fiber with an aperture in the end face. The taper was fabricated by heat-pulling an optical fiber.¹¹ A 220 nm thick aluminum coating was deposited around the fiber to prevent light leakage, which would otherwise add a strong background to the aperture signal. Aluminum was chosen here as it offers the smallest optical penetration depth and thus prevents leakage effectively. Next, the end face of the fiber was cut using focused ion beam (FIB) milling. In contrast to conventional NSOM fibers, the tapered fiber was not cut such that it directly forms a subwavelength aperture. Instead it was cut at a much larger diameter of the taper d_t corresponding to cutoff of the TM₁₁ mode for a specific wavelength.

Panels a–c of Figure 2 show the stages of the fabrication process. The fiber in Figure 2a was cut at a final taper diameter d_t of 370 nm and the end face coated with a 90 nm thick gold film,³⁰ as shown in Figure 2b. The choice of gold as the material for the end face was motivated by its favorable optical properties in the red and infrared where our optical measurements were carried out. In a final step a single subwavelength aperture with diameter d_a was milled into the gold layer, nominally at the center (with a variance of 30 nm in placement). Figure 2c shows a SEM image of an aperture with a diameter of 110 ± 10 nm in the gold-coated end face. Calibration of the milling process ensured that the aperture was milled through the gold layer only and not into the glass fiber core, avoiding spurious effects on the resonance.³¹ Apertures with diameters as small as 45 nm were fabricated, which is well within the cutoff regime where Bethe's theory is typically applied. Several different diameter fiber probes were fabricated by this method, with the glass core diameter d_t ranging from 400 to 730 nm (Figure 2d–f).

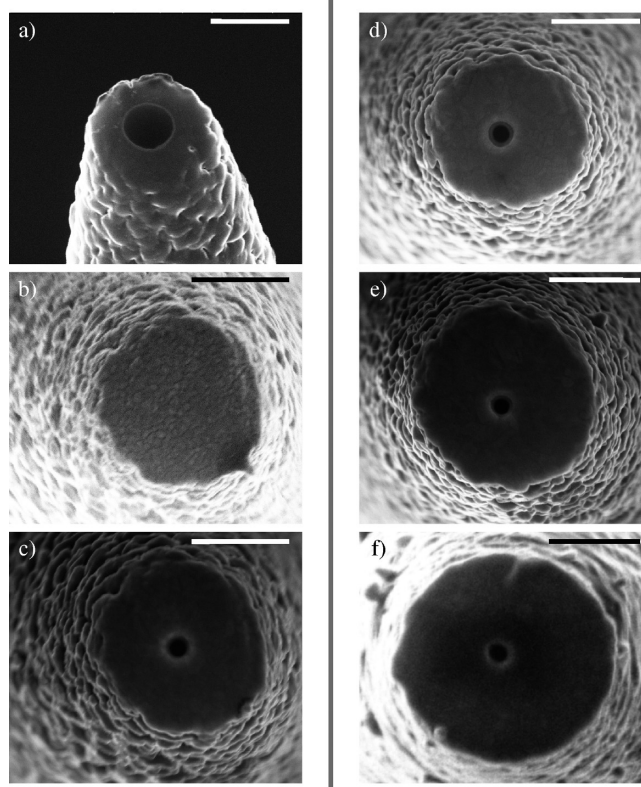


Figure 2. The SEM images in the left column show the three fabrication steps of an EOT near-field fiber probe. (a) The aluminum-coated fiber is cut by focused ion beam (FIB) milling at the desired taper diameter d_t , here 370 nm, which determines the wavelength of the TM mode cutoff. (b) A gold layer of 90 nm is deposited on the end face. (c) Again by FIB, we mill the final aperture into the gold layer. The diameter of the aperture d_a is held constant at 110 ± 10 nm in all fiber probes. The images in the right column show how the overall diameter of the probe as the sum of the taper diameter and coating increases while the taper diameter is varied to achieve different cutoffs of the resonant TM mode. The presented fiber probes have taper diameters of (d) 420 nm, (e) 525 nm, and (f) 724 nm. The scale bar is 500 nm.

The relative transmission of the fabricated enhanced NSOM probes and, for comparison, also of conventional NSOM probes is shown for various aperture diameters in Figure 3. The throughput was determined by coupling light with known intensity at a wavelength of 647 nm into the fiber and recording the transmitted intensity with a large photodetector placed in very close proximity to the fiber end with the aperture. As variations in the taper shape of these probes can have spurious effects on the transmission data, we recorded the throughput of some of the tapered probes first in conventional NSOM configuration; afterward, we processed these probes into the enhanced configuration and recorded the throughput again.

Figure 3 clearly shows the roughly 2 orders of magnitude improved transmission for enhanced probes compared to conventional fiber aperture probes. For a typical aperture size of around 100 nm, the throughput in the resonant configuration was determined to be 10^{-3} , while conventional NSOM probes showed a throughput of approximately 10^{-5} .^{11,12} The enhanced configuration allows a reduction in aperture diameter to as little as 45 nm, while still yielding a throughput of $\sim 10^{-5}$.

To provide a more quantitative comparison with the experimental results, as well as further insight into the underlying

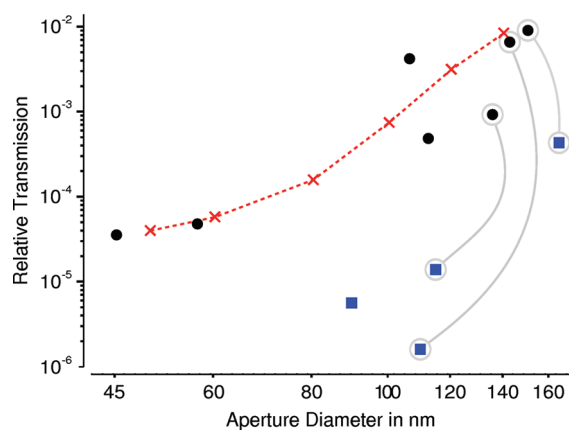


Figure 3. The figure shows the relative transmission as a function of the aperture diameter at a wavelength of 647 nm. The transmission in the enhanced configuration (circles) is 2 orders of magnitude larger than for conventional NSOM probes (squares) for comparable aperture sizes and agrees well with our numerical simulations (crosses, line is guide for the eye). The simulated throughput is fitted to the experimental data in order to account for losses not included in the simulations. Some of the fiber probes were first fabricated as conventional NSOM probes and then processed into the enhanced configuration; data points belonging to the same probe are connected by gray lines.

physics of WR-EOT, comprehensive finite-difference time domain (FDTD) simulations were performed. For these simulations, a mode source with TE_{11} mode profile was incident on the aperture from inside the fiber and the transmission through the gold film and aperture was measured. Perfectly matched layers were placed far enough from the fiber to ensure no spurious effects from coupling to evanescent waves, as confirmed by convergence studies. Convergence studies were also performed on the mesh size to ensure that the impact of plasmonic effects associated with penetration into the metals was accurately captured. We correct for any losses that were not included in the simulations by fitting the simulated relative throughput to the absolute values in the experimental data. As shown in Figure 3, the simulated throughput values for smaller aperture sizes follow nicely the same trend as the experimental values. In particular, the optical transmission for a 50 nm aperture in our setup is still significantly larger than for a 100 nm aperture in a conventional NSOM probe with a 10° taper angle. Therefore, 2 orders of magnitude enhancement in the coupling throughput of the laser power or equivalently a reduction in aperture diameter by over a factor 2 while maintaining the excitation power is achieved with this configuration.

The brightness of conventional aperture probes is in practice limited by their damage threshold that restricts the high power needed to compensate for the low throughput. For our novel probe design, with a higher throughput, one would expect less heat to be absorbed by the coating and thus a higher damage threshold. To investigate the threshold, we coupled light into the fiber and recorded the transmitted power up to damage simultaneously with the power at the fiber launch. As the fiber is tapered, the coupling efficiency at the fiber launch into a propagating fiber mode and thus the absolute power coupled into the fiber cannot be determined with full accuracy. Therefore, once threshold was reached and the aperture is destroyed, we removed the tapered region of the fiber. The damage threshold was then defined as the recorded intensity inside the fiber and above the taper at which the aperture is destroyed.¹³ For the fiber in Figure 2e, with an

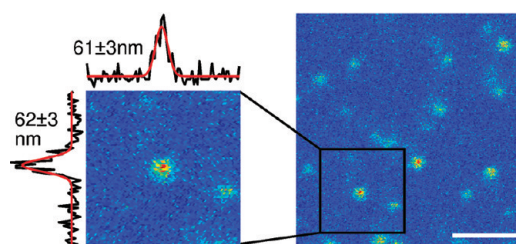


Figure 4. A scan across single TDI molecules with an enhanced NSOM probe with an aperture diameter of 45 nm reveals the improved resolution. The molecules were embedded in a PPMA matrix and were excited at a wavelength of 647 nm. The spatial width of the fluorescence spot is 61 ± 3 and 62 ± 3 nm, respectively. The scale bar is 500 nm.

aperture diameter of 105 nm, we measured the damage threshold to be 8 mW inside the fiber, or, assuming a typical coupling efficiency for NSOM setups of 5%, 160 mW at the launch. For comparison, the conventional aperture probes have a damage threshold of typically less than 0.2 mW inside the fiber or, equivalently, less than 4 mW at the launch. Therefore, the presented configuration improves the damage threshold by approximately $40\times$. We explain this improved damage threshold by a combination of reduced absorption due to an enhanced coupling efficiency and lower optical intensities due to the broader probe design and the cutoff of the lowest order mode, effectively reducing the heat load on the metal coating.

We have measured the performance of the enhanced probe configuration in a home-built NSOM setup on single fluorescent molecules. TDI molecules dissolved in toluene/PMMA solution were spin coated on a glass slide and excited through the near-field of the fiber probe at a wavelength of 647 nm. The fiber probe was scanned over the sample with nanometric accuracy and the fluorescence signal of single molecules recorded with an avalanche photodetector. Figure 4 shows fluorescence measurements of single TDI molecules. The fluorescence spot shows a confinement to 61 ± 3 nm (FWHM), which is close to the aperture diameter of 45 ± 10 nm, as determined from SEM images of this specific fiber. The slightly larger size of the fluorescence spot is attributed to the penetration of the electric field into the gold film, which increases the effective aperture size, and to the finite aperture–molecule distance.

So far, we have assumed that the observed increase in throughput and damage threshold was a sole effect of the absence of a subwavelength taper in this probe design. However, what is the contribution of the WR-EOT? In an effort to determine its effect, we measured the out-coupling transmission and the in-coupling collection spectrum of the probe with both a supercontinuum and a thermal source. These two different configurations yielded nearly identical transmission spectra, when normalized to the light source and detection efficiency. Due to the brightness of the supercontinuum source, the results for the out-coupling transmission spectrum are presented here. For comparison, the transmission spectra of the fibers before the gold coating were also measured. In addition, comparison was made with conventional tapered NSOM aperture probes with the same final aperture diameter.

Figure 5a shows typical measured and simulated transmission spectra of two of the fabricated fiber probes. As the reported EOT phenomena is associated with mode cutoff in the fiber waveguide, we expect the longest-wavelength peak to result from EOT and thus to depend on the final taper diameter.

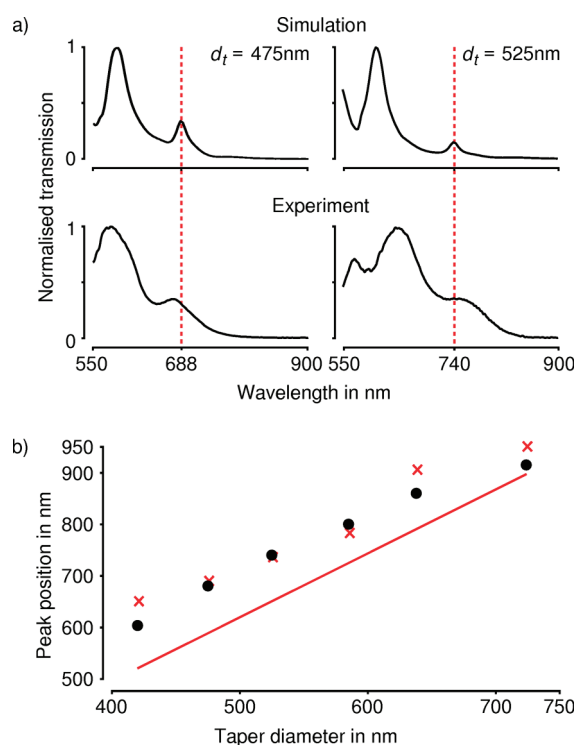


Figure 5. (a) Simulations (top row) and experimentally recorded transmission spectra (bottom row), are shown exemplary for two fiber probes with final taper diameters d_t of 475 nm (left column) and 525 nm (right column). The dashed lines indicate the transmission peak where the TM_{11} mode at cutoff in the tapered fiber waveguide couples resonantly to the aperture and extraordinary transmission is observed. (b) The spectral positions of the transmission peaks attributed to mode cutoff. The numerical simulations (crosses) are in good agreement with the experimental data (circles) and confirm the existence of the waveguide resonant extraordinary optical transmission. Indicated by the red line is the cutoff wavelength corresponding to the TM_{11} mode as predicted by eq 1 for a perfect electric conductor.

This assumption is confirmed as an almost linear dependence between final taper diameter and peak position is clearly visible in Figure 5b. Each fiber probe shows a distinct transmission peak that shifts to longer wavelengths with increasing diameter of the taper, and the calculations show good quantitative agreement with the measurements in the location of the resonances in Figure 5a.

This peak in transmission is the result of WR-EOT. The WR-EOT occurs for wavelengths above the cutoff of one of the higher-order TM modes in the waveguide. Approaching the cutoff, the admittance of that waveguide mode diverges, as does the admittance of the aperture as it is made infinitesimally small. Therefore, the transmission phenomenon may be considered as a problem of impedance matching, where the energy builds up resonantly in the TM mode above its cutoff. This phenomenon is similar to EOT in aperture arrays, where surface waves store the energy to allow for enhanced transmission at wavelengths longer than the Wood's anomaly;¹⁷ except here, only a single aperture is present. A criterion for WR-EOT is that the mode inside the fiber has a divergent transverse magnetic field at its cutoff wavelength, which enhances the coupling to the aperture through Bethe's theory.²⁶ Various TM modes may be chosen to satisfy these criteria; however, the TM_{11} mode was selected in this case because it is the lowest order mode that allows for concentric apertures (i.e., it has a nonzero transverse

magnetic field in the center of the waveguide).²⁷ This cutoff mode inside the fiber is evanescent away from the metal film at the NSOM tip; therefore, it is equivalent to a surface wave, and its energy is stored near the surface with the aperture. This is analogous to the surface waves in EOT of hole arrays, except that here the geometry of the fiber replaces the periodicity of the array. The mode cutoff, which is analogous to the Wood's anomaly wavelength in the array case, is given by³²

$$\lambda_c = \frac{\pi d_t n_f}{3.832} \quad (1)$$

where n_f is the refractive index of the fiber, d_t is the final taper diameter, and it is assumed for simplicity that the aluminum coating is a perfect electric conductor. Figure 5b shows the location of the cutoff predicted by this equation as a red line. Indeed eq 1 describes the trend, yet it is clear that the peak resonant transmission occurs for wavelengths slightly longer than the cutoff of the TM_{11} mode.

As emphasized above, the TM_{11} cutoff mode plays a critical role in the WR-EOT as it stores energy at the resonant peak, and it is crucial to verify that the resonant peak corresponds to a TM_{11} mode profile inside the fiber, within the decay length of the cutoff mode. Figure 6a shows numerical simulations of the z -component of the electric field inside the two fiber probes adjacent to the gold-coated end face at the resonance wavelength of 648 and 688 nm for the fibers with taper diameter d_t of 420 and 475 nm, respectively. The field distribution, shown 150 nm inside the fiber, matches that of the TM_{11} . In Figure 6b we have also monitored the field at two interfaces and at the center of the aperture. These have very similar field intensity profiles, represented by the enhanced field confined to the aperture region, with a dominant resonant background from the TM_{11} mode. To distinguish our excitation mode from the TM_{11} cutoff mode, we also monitored the Poynting vector (obtained by the cross product of the transverse electric and magnetic fields) 150 nm inside the fiber in Figure 6a. As expected, the Poynting vector profile is predominantly the TE_{11} mode, which is the propagating mode by which we excite the fiber. Fabrication margins and a resulting small offset of the aperture on the end face were included in the simulations and cause the slight asymmetry of the field distribution. For wavelengths 100 nm below and above the resonance wavelength, the resonance is $10\times$ weaker. Experimentally, in Figure 5a we observed a 2- to 3-fold increase in intensity at the resonance wavelengths compared to the non-resonant contribution in the spectra.

The $100\times$ total improvement in throughput over a conventional NSOM fiber probe is due to the effect of EOT and an increase in magnitude of the electric field arriving at the aperture, with both being a consequence of carefully nanostructuring the probe. The absence of a strongly attenuating subwavelength taper, present in conventional NSOM fiber probes, improves the coupling through the taper region to the aperture, effectively increasing the magnitude of the electric field at the aperture; the effect of EOT is to enhance the coupling through the subwavelength aperture itself. As the shape of the subwavelength taper and thus the strength of the attenuation depend strongly on the fabrication parameters, its absence in the enhanced configuration also improves the fabrication yield as compared to conventional probes. The challenge of matching the probe dimensions to a specific wavelength depends merely on the quality of the nanofabrication.

In conclusion, we have experimentally demonstrated a novel, efficient near-field probe that shows an improvement of a

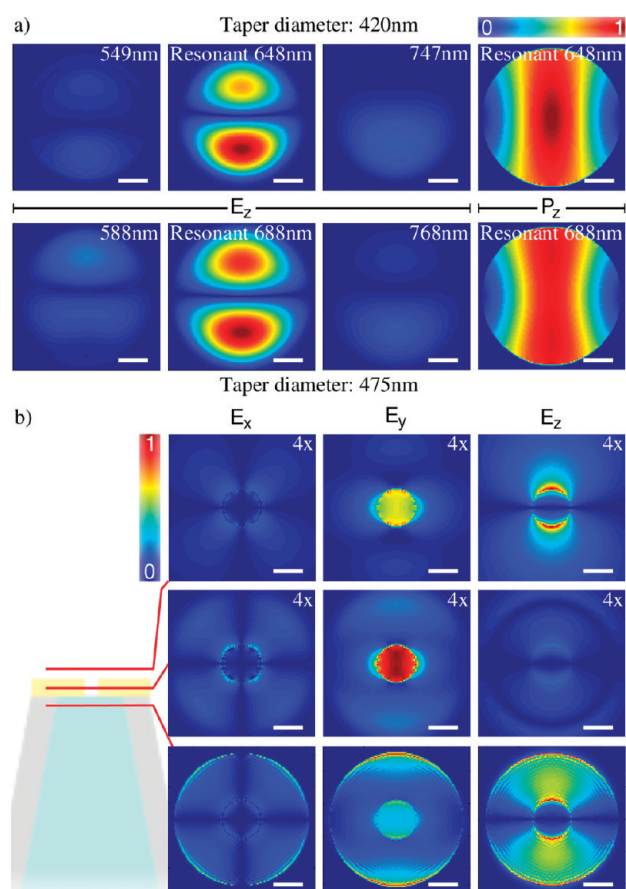


Figure 6. (a) The z -component of the electric field (E_z) at 150 nm from the gold surface inside the fiber matches the field distribution expected of a TM_{11} mode for the fiber in Figure 2d (diameter 420 nm, top) and Figure 2e (diameter 525 nm, bottom), with some asymmetry from the offset of the aperture from the middle (included in the simulations). The field intensity is $10\times$ greater at the resonant wavelength than at a nonresonant wavelength. The Poynting vector (P_z) at the same position matches the profile of the TE_{11} mode by which we excite the fiber. All electric fields are normalized to the respective resonant case, and the Poynting vector is normalized to 1. (b) The electric field components E_x , E_y , and E_z above, inside, and beneath the aperture are normalized to the same strongest field component for easy comparison. The scale bar is 100 nm.

$40\times$ enhanced damage threshold and a $100\times$ enhanced throughput over conventional tapered fiber probes. We have realized aperture probes of only 45 nm in diameter and successfully imaged single molecules with this resolution, which confirms the subwavelength confinement of the transmitted light and the practicality of the probes for near-field scanning optical microscopy. Contributing to the high probe efficiency is a new type of EOT that relies solely on the coupling between the fiber waveguide at mode cutoff and the aperture, as confirmed with comprehensive electromagnetic simulations. We have shown that the spectral position of the resonance depends on the cutoff wavelength of the fiber waveguide, so that the peak wavelength could be tuned while maintaining the same aperture size. In the future, smaller diameter WR-EOT probes are envisioned by exploiting the cutoff resonances of lower order modes, as has already been demonstrated in the microwave regime.²⁹

Potential applications that benefit from the high efficiency of the demonstrated NSOM probe include imaging, sensing (Raman scattering³³), nanolithography, and trapping and manipulation of

nanoscale particles, such as viruses.³⁴ EOT on a single aperture has applications in high sensitivity sensing,³⁵ as had been studied extensively in aperture arrays.³⁶ We also believe that this configuration may open up new applications for fiber probes where nonlinear interactions are required, such as with higher-harmonic generation³⁷ or two-photon luminescence.^{38,39}

AUTHOR INFORMATION

Corresponding Author

*E-mail: Niek.vanHulst@icfo.es.

ACKNOWLEDGMENT

This research was funded by the Spanish Ministry of Science and Innovation (MICINN) through programs FIS2009-08203 and CSD2007-046 “NanoLight”, Fundació CELLEX Barcelona, and the European Research Council (NvH, ERC-Advanced Grant). L.N. was partially funded by the Commission for Universities and Research of the Department of Innovation, Universities and Enterprises of the Catalan Government and the European Social Fund. R.G. and Y.P. acknowledge support from the Natural Sciences and Engineering Research Council (NSERC) of Canada Discovery Grant. Y.P. acknowledges support from the Jarmila Vlasta Von Drak Thouvenelle Graduate Scholarship. R.G. acknowledges support from a visiting professorship from the Agència de Gestió d'Ajuts Universitaris I de Recerca (AGAUR), Generalitat de Catalunya.

REFERENCES

- (1) Pohl, D. W.; Denk, W.; Lanz, M. *Appl. Phys. Lett.* **1984**, *44*, 651.
- (2) Betzig, E.; Chichester, R. J. *Science* **1993**, *262*, 1422.
- (3) Yang, P.; Yan, H.; Mao, S.; Russo, R.; Johnson, J.; Saykally, R.; Morris, N.; Pham, J.; He, R.; Choi, H.-J. *Adv. Funct. Mater.* **2002**, *12*, 323.
- (4) Abashin, M.; Tortora, P.; Märki, I.; Levy, U.; Nakagawa, W.; Vaccaro, L.; Herzig, H. P.; Fainman, Y. *Opt. Express* **2006**, *14*, 1643.
- (5) Descrovi, E.; Sfez, T.; Quaglio, M.; Brunazzo, D.; Dominici, L.; Michelotti, F.; Herzig, H. P.; Martin, O. J. F.; Giorgis, F. *Nano Lett.* **2010**, *10*, 2087.
- (6) Michaels, C. A.; Gu, X.; Chase, D.; Stranick, S. J. *Appl. Spectrosc.* **2004**, *58*, 257.
- (7) Betzig, E.; Trautman, J. K.; Wolfe, R.; Gyorgy, E. M.; Finn, P. L.; Kryder, M. H.; Chang, C.-H. *Appl. Phys. Lett.* **1992**, *61*, 142.
- (8) Jersch, J.; Demming, F.; Hildenhagen, L. J.; Dickmann, K. *Appl. Phys. A: Mater. Sci. Process.* **1998**, *66*, 29.
- (9) Sun, S.; Leggett, G. J. *Nano Lett.* **2004**, *4*, 1381.
- (10) Bethe, H. A. *Phys. Rev.* **1944**, *66*, 163.
- (11) Valaskovic, G. A.; Holton, M.; Morrison, G. H. *Appl. Opt.* **1995**, *34*, 1215.
- (12) Veerman, J. A.; Otter, A. M.; Kuipers, L.; van Hulst, N. F. *Appl. Phys. Lett.* **1998**, *72*, 3115.
- (13) Hecht, B.; Sick, B.; Wild, U. P.; Deckert, V.; Zenobi, R.; Martin, O. J. F.; Pohl, D. W. *J. Chem. Phys.* **2000**, *112*, 7761.
- (14) Wang, L.; Uppuluri, S. M.; Jin, E. X.; Xu, X. *Nano Lett.* **2006**, *6*, 361.
- (15) Sundaramurthy, A.; Schuck, P. J.; Conley, N. R.; Fromm, D. P.; Kino, G. S.; Moerner, W. E. *Nano Lett.* **2006**, *6*, 355.
- (16) Onuta, T.-D.; Waegle, M.; DuFort, C. C.; Schaich, W. L.; Dragnea, B. *Nano Lett.* **2007**, *7*, 557.
- (17) Ebbesen, T. W.; Lezec, H. J.; Ghaemi, H. F.; Thio, T.; Wolff, P. A. *Nature* **1998**, *391*, 667.
- (18) Lezec, H. J.; Degiron, A.; Devaux, E.; Linke, R. A.; Martin-Moreno, L.; Garcia-Vidal, F. J.; Ebbesen, T. W. *Science* **2002**, *297*, 820.
- (19) Novotny, L.; Stranick, S. J. *Annu. Rev. Phys. Chem.* **2006**, *57*, 303.

- (20) Gerton, J. M.; Wade, L. A.; Lessard, G. A.; Ma, Z.; Quake, S. R. *Phys. Rev. Lett.* **2004**, *93*, No. 180801.
- (21) Taminiou, T. H.; Moerland, R. J.; Segerink, F. B.; Kuipers, L.; van Hulst, N. F. *Nano Lett.* **2007**, *7*, 28.
- (22) Mivelle, M.; Ibrahim, I. A.; Baida, F.; Burr, G. W.; Nedeljkovic, D.; Charrat, D.; Rauch, J.-Y.; Salut, R.; Grosjean, T. *Opt. Express* **2010**, *18*, 15964.
- (23) de Angelis, F.; Patrini, M.; Das, G.; Maksymov, I.; Galli, M.; Businaro, L.; Andreani, L. C.; di Fabrizio, E. *Nano Lett.* **2008**, *8*, 2321.
- (24) Renna, F.; Cox, D.; Brambilla, G. *Opt. Express* **2009**, *17*, 7658.
- (25) Wang, Y.; Srituravanich, W.; Sun, C.; Zhang, X. *Nano Lett.* **2008**, *8*, 3041.
- (26) Gordon, R. *Phys. Rev. A* **2007**, *76*, No. 053806.
- (27) Medina, F.; Mesa, F.; Marqués, R. *IEEE Trans. Microwave Theory Tech.* **2008**, *56*, 3108.
- (28) Pang, Y.; Hone, A. N.; So, P. P. M.; Gordon, R. *Opt. Express* **2009**, *17*, 4433.
- (29) Medina, F.; Ruiz-Cruz, J. A.; Mesa, F.; Rebolgar, J. M.; Montejo-Garai, J. R.; Marqués, R. *Appl. Phys. Lett.* **2009**, *95*, No. 071102.
- (30) Gérard, D.; Wenger, J.; Bonod, N.; Popov, E.; Rigneault, H.; Mahdavi, F.; Blair, S.; Dintinger, J.; Ebbesen, T. W. *Phys. Rev. B* **2008**, *77*, No. 045413.
- (31) Kang, J. H.; Choe, J.-H.; Kim, D. S.; Park, Q.-H. *Opt. Express* **2009**, *17*, 15652.
- (32) Pozar, D. M. *Microwave Engineering*; Wiley: Hoboken, NJ, 2004.
- (33) Richards, D.; Milner, R. G.; Huang, F.; Festy, F. *J. Raman Spectrosc.* **2003**, *34*, 663.
- (34) Juan, M. L.; Gordon, R.; Pang, Y.; Eftekhari, F.; Quidant, R. *Nat. Phys.* **2009**, *5*, 915.
- (35) Wenger, J.; Gérard, D.; Aouani, H.; Rigneault, H.; Lowder, B.; Blair, S.; Devaux, E.; Ebbesen, T. W. *Anal. Chem.* **2009**, *81*, 834.
- (36) Brolo, A. G.; Gordon, R.; Leathem, B.; Kavanagh, K. L. *Langmuir* **2004**, *20*, 4813.
- (37) Johnson, J. C.; Yan, H.; Schaller, R. D.; Petersen, P. B.; Yang, P.; Saykally, R. J. *Nano Lett.* **2002**, *2*, 279.
- (38) Sanchez, E. J.; Novotny, L.; Xie, X. S. *Phys. Rev. Lett.* **1999**, *82*, 4014.
- (39) Imura, K.; Okamoto, H. *J. Phys. Chem. C* **2009**, *113*, 11756.